THE JOURNAL OF BIOLOGICAL CHEMISTRY VOL. 288, NO. 35, pp. 25219–25228, August 30, 2013

Calcium Ions Promote Superoxide Dismutase 1 (SOD1) Aggregation into Non-fibrillar Amyloid

*A LINK TO TOXIC EFFECTS OF CALCIUM OVERLOAD IN AMYOTROPHIC LATERAL SCLEROSIS (ALS)?**

Received for publication, March 20, 2013, and in revised form, June 20, 2013 Published, JBC Papers in Press, July 16, 2013, DOI 10.1074/jbc.M113.470740

Sónia S. Leal[‡], **Isabel Cardoso**[§], **Joan S. Valentine**[¶], **and Cláudio M. Gomes**[‡1]

From the [‡]*Instituto Tecnologia Química e Biológica, Universidade Nova de Lisboa, Av. República 127, 2780-756 Oeiras, Portugal, the* [§]*Molecular Neurobiology Unit, Instituto Biologia Molecular e Celular, 4150-180 Porto, Portugal, and the* [¶]*Department of Chemistry and Biochemistry, UCLA, Los Angeles, California 90095*

Background: SOD1-enriched protein inclusions and Ca^{2+} overload are hallmarks in ALS-affected motor neurons. Ca^{2+} burden correlates with SOD1 aggregation in cellular models.
Results: Ca^{2+} induces conformational changes that enhance and shift SOD1 aggregation from fibrils toward amorphous aggregates.
Conclusion: SOD1 aggregation is enhanced and modulated by Ca^{2+}.
Significance: Ca^{2+} can behave as a pathogenic effector in the formation of ALS proteinaceous inclusions.

Imbalance in metal ion homeostasis is a hallmark in neurodegenerative conditions involving protein deposition, and amyotrophic lateral sclerosis (ALS) is no exception. In particular, Ca^{2+} dysregulation has been shown to correlate with superoxide dismutase-1 (SOD1) aggregation in a cellular model of ALS. Here we present evidence that SOD1 aggregation is enhanced and modulated by Ca^{2+}. We show that at physiological pH, Ca^{2+} induces conformational changes that increase SOD1 β-sheet content, as probed by far UV CD and attenuated total reflectance-FTIR, and enhances SOD1 hydrophobicity, as probed by ANS fluorescence emission. Moreover, dynamic light scattering analysis showed that Ca^{2+} boosts the onset of SOD1 aggregation. In agreement, Ca^{2+} decreases SOD1 critical concentration and nucleation time during aggregation kinetics, as evidenced by thioflavin T fluorescence emission. Attenuated total reflectance FTIR analysis showed that Ca^{2+} induced aggregates consisting preferentially of antiparallel β-sheets, thus suggesting a modulation effect on the aggregation pathway. Transmission electron microscopy and analysis with conformational anti-fibril and anti-oligomer antibodies showed that oligomers and amyloidogenic aggregates constitute the prevalent morphology of Ca^{2+}-induced aggregates, thus indicating that Ca^{2+} diverts SOD1 aggregation from fibrils toward amorphous aggregates. Interestingly, the same heterogeneity of conformations is found in ALS-derived protein inclusions. We thus hypothesize that transient variations and dysregulation of cellular Ca^{2+} levels contribute to the formation of SOD1 aggregates in ALS patients. In this scenario, Ca^{2+} may be considered as a pathogenic effector in the formation of ALS proteinaceous inclusions.

Amyotrophic lateral sclerosis (ALS)[2] is a fatal neurodegenerative disease characterized by the selective degeneration of motor neurons in the spinal cord, brainstem, and cerebral cortex (1). Most cases of ALS are sporadic with no known genetic linkage, whereas ~10% are associated with familial causes (fALS). Both forms share a similar neurodegeneration pattern and are clinically and pathologically indistinguishable (2), thus suggesting a common molecular mechanism. One of the common features in all ALS patients is the presence of cytoplasmic proteinaceous aggregates in motor neurons, suggested to play a determinant role in neuron toxicity, degeneration, and cell death (3–7). In this respect, inclusions enriched in mutant variants of superoxide dismutase-1 (SOD1) are a well established hallmark of fALS-SOD1-associated forms of the disease (7–11). However, sporadic ALS patients also contain wild type SOD1 in proteinaceous inclusions (12–15), which share aberrant conformations of mutant SOD1 clinical variants that are known to cause aggregation (16–18). In fact, expression of recombinant peptide fragments of wild type SOD1 in cultured cells results in insoluble fALS-SOD1-like conformers, suggesting that SOD1 is inherently prone to aggregate (19). Therefore, fALS mutations and environmental adverse conditions are probably triggers of SOD1 toxic aggregation, which seems to be an intrinsic property of this protein. Thus, wild type SOD1 is suggested to be involved in ALS pathology (20, 21), inducing toxicity that degenerates motor neurons (22).

SOD1 is a highly stable homodimeric protein that holds in each monomer a disulfide bridge as well as a copper/zinc binuclear site. Interestingly, SOD1 aggregates from a transgenic fALS mouse model tend to be metal-deficient and/or lack the disulfide bond (23, 24), raising the possibility that disease-causing mutations may deregulate and increase levels of SOD1

* This work was supported by the Fundação para a Ciência e Tecnologia (FCT/MCTES, Portugal) through Research Grants PTDC/QUI-BIQ/117789/2010 and PTDC/EBB-BIO/117793/2010 (to C. M. G.), Postdoctoral Fellowship SFRH/BPD/47477/2008 (to S. S. L.), and Strategic Grant PEst-OE/EQB/LA0004/2011 (to the Instituto Tecnologia Química e Biológica Laboratório Associado).
[1] To whom correspondence should be addressed. Tel.: 351-214469332; Fax: 351-214411277; E-mail: gomes@itqb.unl.pt.

[2] The abbreviations used are: ALS, amyotrophic lateral sclerosis; fALS, familial ALS; ThT, thioflavin T; SOD, superoxide dismutase; ATR, attenuated total reflectance; ANS, 1-anilino-8-naphthalenesulfonate; DLS, dynamic light scattering; TEM, transmission electron microscopy.

immature conformers. In agreement, the folding pathway of SOD1 clinical mutants has been suggested to favor the accumulation of metal-depleted (apo) monomeric intermediates (25), which are prone to aggregate (26–28). In fact, post-translational modifications are major structural determinants for SOD1 stability (29, 30). Each SOD1 chain folds into a β-barrel that is flanked by two major loops, the zinc and the electrostatic loops, which together shape the active site. In the absence of metal coordination, the β-barrel and dimer interface remain intact, but the associated loops become highly disordered (31–33). Further, reduction of the native disulfide bridge promotes dimer dissociation, yielding monomers with a high level of conformational flexibility (34, 35).

Immature SOD1 states alone are, however, insufficient to explain SOD1-linked ALS pathogenesis; not all ALS-related SOD1 variants evidence increased destabilization of the apo state (36) and reduced apo state (37) with respect to the wild type form. Thus, additional chemical and biological factors must account for the toxicity of SOD1 in ALS. One lead arises from the fact that, although ubiquitously expressed in all tissues (38, 39), SOD1 only aggregates within specific motor neurons in ALS. This preferential vulnerability suggests that unique properties within the affected neurons, besides SOD1 mutations, are likely to be mandatory for the onset of SOD1 aggregation. One such characteristic within the affected motor neurons is a vulnerability to calcium overload; indeed, these cells express highly calcium-permeable AMPA receptors (40–44) with concurrent low calcium buffering capacity due to a lack of the Ca^{2+}-buffering proteins parvalbumin and calbindin (45, 46). In agreement, calcium ions accumulate in the spinal and brain stem motor neurons of ALS patients as well as in animal and cell models of ALS-SOD1 (47–53). Moreover, studies on these models have shown that Ca^{2+} overload promotes and correlates with SOD1 aggregation (54, 55). Interestingly, oculo-motor neurons, which are not affected in ALS, have a 5–6-fold higher Ca^{2+} buffering capacity than the spinal and brain stem ALS-vulnerable motor neurons (56). This particular observation suggests that Ca^{2+} may be a key factor in modulating SOD1 toxicity in ALS; indeed, endogenous Ca^{2+} levels are systematically elevated in the specific motor neurons in which SOD1 proteinaceous aggregates are found. In this study, we have thus addressed *in vitro* the effect of this metal ion on the aggregation mechanism of SOD1, and the results obtained suggest a link between elevated Ca^{2+} levels and SOD1 aggregation in ALS.

MATERIALS AND METHODS

Chemicals and Sample Preparation—All reagents were of the highest grade commercially available. SOD1 was expressed in *E. coli* BL21(DE3) strain and grown and purified as described (57). All SOD1 experiments were performed using the demetallated form (apo-SOD1). The preparation of apo-SOD1 was obtained following published procedures (58). Metal content of apo-SOD1 was confirmed using the colorimetric reagent Zincon (59). A Chelex resin (Bio-Rad) was used to remove contaminant trace metals from all buffer solutions and to maintain apo-SOD1 in the demetallated form. Concentration of SOD1 was determined using the extinction coefficient 10,800 cm^{-1} M^{-1} at 280 nm. The broad range of concentrations used throughout biophysical experiments relates to the specific requirements and limitations of each of the different techniques used.

Circular Dichroism (CD)—Far UV CD analyses were performed using a Jasco J-815 spectropolarimeter equipped with a Peltier-controlled thermostated cell support. CD spectra were the average of eight scans obtained by collecting data at 0.1 nm intervals from 260 to 190 nm. The results were expressed as mean residue molar ellipticity $[\theta]$ with units of degrees cm^2/dmol, as calculated from the equation,

$$[\theta] = ([\theta]_{obs} \times MRW)/(10 \times c \times l) \quad \text{(Eq. 1)}$$

where $[\theta]_{obs}$ is the ellipticity measured in millidegrees, MRW is the mean residue molecular weight, c is the protein concentration in mg/ml, and l is the optical path length of the cell in cm. Spectra were recorded with 30 μM apo-SOD1 samples in 50 mM Tris, pH 7.5, that were previously incubated overnight with increasing concentrations of $CaCl_2$ at 37 °C and 600 rpm.

ATR-FTIR—Infrared spectra were performed on a Bruker IFS 66/S spectrometer equipped with a mercury/cadmium/telluride (MCT) infrared detector and a thermostatized Harrick BioATR II cell. All measurements were obtained in an ATR cell with 150 μM apo-SOD1 and 300 μM SOD1 aggregates at pH 7.5 formed in the absence and presence of 300 and 600 μM $CaCl_2$, respectively. Each spectrum comprises the mean of 150 scans taken at a resolution of 2 cm^{-1}. Spectra were corrected for the buffer and water vapor. Difference absorption spectra are the average of independent subtractions between three data sets of Ca^{2+}-incubated and control samples. The 1750–1700 cm^{-1} region is shown to demonstrate the absence of major contributions from noise or water vapor artifacts, thus validating the data. Region assignments were based on typical absorption regions for specific secondary structure elements (60).

ANS Binding Assay—ANS fluorescence emission enhancement was evaluated in a BMG Fluostar Optima fluorescence plate reader using a 370-nm excitation filter and a 480-nm emission filter. Samples of 15 μM apo-SOD1 were prepared as triplicates in 50 mM Tris, pH 7.5, that were previously incubated overnight with increasing concentrations of $CaCl_2$ at 37 °C and 600rpm in black 96-well plates (Nunc, catalog no. 732-2701). The ANS fluorescence emission spectrum was recorded in a Cary Varian Eclipse instrument possessing a Peltier-thermostated cell support.

Dynamic Light Scattering (DLS)—DLS measurements were carried out in a Malvern Zetasizer Nano ZS instrument equipped with a 4-megawatt helium-neon laser (632 nm). 60 μM apo-SOD1 samples in 50 mM Tris, pH 7.5, were incubated with different concentration ratios of $CaCl_2$/SOD1, filtered through a 0.45-μm filter, and incubated overnight at 37 °C and 600 rpm before DLS analyses. A $CaCl_2$/SOD1 molar ratio of 2 was used to compare the mean light scattering intensity variation over time with control. After 24, 48, 68, and 90 h of incubation, 50-μl aliquots were collected and measured in a 45-μl quartz cuvette (Hellma) at 37 °C. The operating procedure was set to 17 runs, each being averaged for eight measurements. The resulting data were analyzed using DTS (version 6.32) software (Malvern).

Thioflavin T Fluorescence Binding—Real-time ThT fluorescence (480 nm) was recorded using a BMG Fluostar Optima

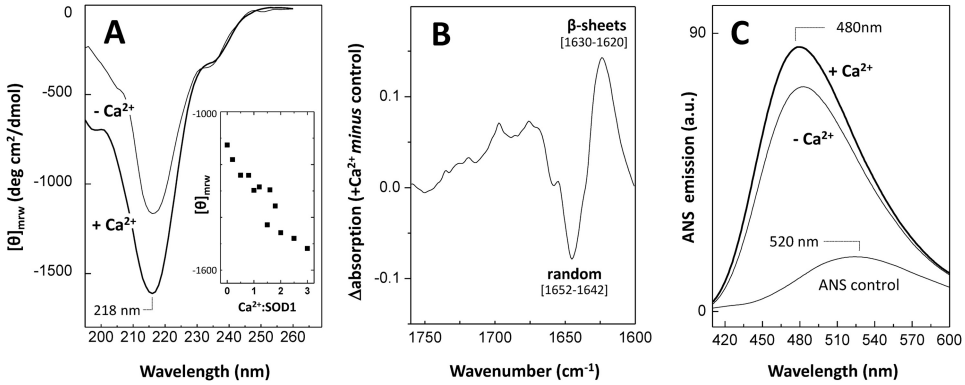

FIGURE 1. **Effect of Ca^{2+} on the secondary structure and hydrophobicity of apo-SOD1.** *A*, far UV CD spectra of apo-SOD1 ($-Ca^{2+}$) and upon overnight incubation with Ca^{2+} ($+Ca^{2+}$) *Inset*, plot of the intensity of the SOD1-negative band centered at 218 nm, at increasing Ca^{2+}/SOD1 ratios. *B*, ATR-FTIR difference spectrum in the amide I region of Ca^{2+}-incubated SOD1 minus the control; positive peaks denote features increased in the presence of Ca^{2+}. *C*, ANS fluorescence emission spectra of apo-SOD1 ($-Ca^{2+}$) and upon incubation with Ca^{2+} ($+Ca^{2+}$), overlaid with the emission spectrum of unbound ANS. See "Materials and Methods" for further details.

fluorescence plate reader upon excitation at 440 nm. Readings were taken every 7 min, and the well plates were subjected to 5 min of agitation at 600 rpm prior to each fluorescence measurement. Assays were performed in black 96-well plates (Nunc, catalog no. 732-2701). Samples were prepared as triplicates at a wide range of concentrations of apo-SOD1 (20–120 μM) with and without adding $CaCl_2$ up to a molar ratio of Ca^{2+}/SOD1 = 2 and mixed with a 2× molar ratio of ThT in 50 mM Tris, pH 7.5, at 37 °C. Final sample volume in each lane was 200 μl, and all wells contained one Teflon bead (⅛-inch diameter). Aggregation curve analyses were performed by fitting the data to the equation,

$$Y = (y_i + m_i x) + \frac{(v_f + m_i x)}{\left(1 + \exp^{-\left(x - \frac{X_0}{\tau}\right)}\right)} \qquad \text{(Eq. 2)}$$

where Y corresponds to fluorescence intensity, x is the time, and X_0 corresponds to the time of half-height of fluorescence intensity (t_{50}). The lag phase is calculated by $t_{lag} = X_0 - 2\tau$, and the apparent rate velocity (k_{app}) = $1/\tau$. Kinetic parameters have been determined from six independent determinations.

Dot Blotting Using Amyloid Conformational Antibodies—10 μl of SOD1 aggregates obtained at the plateau phase of each aggregation kinetic curve were dotted in triplicates onto PVDF membranes and probed with a 1:500 dilution of the anti-amyloid oligomer A11 antibody (AB9234, Merck Millipore) and 1:1000 for the anti-amyloid fibril OC antibody (AB2286, Merck Millipore) according to the manufacturer's instructions. Dots were visualized using a horseradish peroxidase-conjugated IgG secondary antibody with a chemiluminescence detection system (GE Healthcare). Images were recorded and analyzed using Quantity One analysis software from Bio-Rad.

Transmission Electron Microscopy—For visualization by TEM, 5 μl of 300 μM apo-SOD1 aggregates formed with and without adding $CaCl_2$ up to a molar ratio of Ca^{2+}/SOD1 = 2 were absorbed to carbon-coated collodion film supported on 400-mesh copper grids and negatively stained with 1% uranyl acetate. The grids were exhaustively visualized with a Jeol microscope (JEM-1400), operated at 80 kV.

RESULTS

Calcium Increases Apo-SOD1 β-Sheet Content and Hydrophobicity—We have started by investigating if Ca^{2+} has an effect on SOD1 native structure. This follows the evidence that protein aggregation does not necessarily require the formation of an unfolded conformer but may rather result from dynamic fluctuations around the native state, due to environmental variations, disruption of post-translation interactions, or mutations (61). In particular, we focused on effects on β-sheet structures and hydrophobicity changes because these properties are often altered in aggregation-prone conformers (62). The effects of increasing Ca^{2+} concentration on SOD1 secondary structure were investigated using far UV circular dichroism (Fig. 1*A*). We observed that incubation of the protein with $CaCl_2$ at up to a molar ratio of Ca^{2+}/SOD1 of 3 results in a roughly linear change of the signal of the negative band centered at 218 nm (Fig. 1*A*, *inset*), thus suggesting a direct correlation between the presence of Ca^{2+} and an increased content of SOD1 β-sheets. In a control experiment using NaCl, no change was observed. The impact of Ca^{2+} on SOD1 secondary structure was further analyzed by ATR-FTIR analysis. Indeed, the difference FTIR absorption spectrum in the amide I region, obtained from subtracting the Ca^{2+} incubated from the control SOD1 sample, also reveals secondary structure changes. An increase in β-sheet content (positive amplitude bands in the 1620–1630 cm^{-1} region) is observed alongside a decrease in randomness (negative amplitude bands in the 1642–1652 cm^{-1} region) (Fig. 1*B*). The observed variations are thus suggestive of conformational rearrangements taking place in the presence of Ca^{2+}.

To verify if Ca^{2+} also promotes alterations on SOD1 hydrophobicity, we have used ANS, a fluorophore that interacts with exposed hydrophobic patches within β-sheeted structures (63). ANS is scarcely fluorescent when free in an aqueous neutral solution, emitting at 520 nm (Fig. 1*C*, *trace a*). However, a blue shift to around 480 nm as well as an increase in intensity of fluorescence emission are observed upon ANS binding to hydrophobic surfaces in proteins (64). In agreement with previous reports, apo-SOD1 binds ANS (Fig. 1*C*, *trace b*) (65); however, the presence of Ca^{2+} results in a ~15% increase in ANS

fluorescence emission (Fig. 1*C*, *trace c*). The intensity of ANS fluorescence emission was found to increase up to an excess molar ratio of Ca^{2+}/SOD1 of 2. For higher molar ratios of Ca^{2+}, the ANS emission tends to decrease, suggesting that fewer hydrophobic moieties are accessible (not shown). This could be an indication that intermolecular hydrophobic interactions are being formed at higher Ca^{2+} concentrations, thus decreasing the exposed hydrophobic regions available for ANS binding. This would be compatible with an oligomerization process through structural reorganization involving hydrophobic burial (66). Overall, the results indicate that in the presence of Ca^{2+}, SOD1 adopts distinct conformational states that are β-sheet-enriched.

Calcium Promotes Oligomerization and Conformational Heterogeneity of Apo-SOD1—In order to investigate a possible link between the ANS results and the formation of intermolecular interactions at increasing Ca^{2+} concentrations, we have used DLS, a very sensitive technique for assessing changes in the oligomerization state of protein solutions (67). After 24 h of incubation at 37 °C and constant agitation, a monomodal size distribution profile by volume with a mean peak averaging at a hydrodynamic diameter of ~5.4 ± 0.4 nm was observed for all samples, irrespective of the presence of Ca^{2+} up to a molar ratio of 4. However, the absence of a multimodal distribution by volume in DLS does not necessarily imply the absence of aggregates if the population of formed oligomeric species is very low relative to that of dimeric SOD1 (68, 69). We have thus probed for oligomeric species by comparing the mean hydrodynamic diameter (*Z*-average size), a parameter extremely sensitive to the presence of minor populations of larger oligomers, as well as the mean count rate parameter for evaluation of the scattering intensity. From this combined analysis, we determined an increase in the mean hydrodynamic diameter for the Ca^{2+}-incubated SOD1 samples, from 6.5 ± 0.3 nm for the control to 7.9 ± 0.9, 10.1 ± 1.5, and 10.1 ± 2.5 nm for samples at Ca^{2+}/SOD1 molar ratios of 1, 2, and 4, respectively. An increase in mean light scattering intensity was also observed upon increasing concentrations of added Ca^{2+}, from 356 ± 18 nm for the control, to 377 ± 10, 439 ± 26, and 543 ± 31 nm for samples at Ca^{2+}/SOD1 ratios of 1, 2, and 4, respectively. The results suggest a correlation between increasing Ca^{2+}/SOD1 ratios and enhanced oligomerization (Fig. 2), in agreement with Ca^{2+} inducing aggregation and conformational heterogeneity on SOD1. The used Ca^{2+} concentrations (60–240 μM) bear some resemblance to physiological ones because intracellular micromolar transients of free Ca^{2+} are known to occur *in vivo* upon neuron stimulation (70–72).

Calcium Enhances Apo-SOD1 Aggregation—In order to further characterize the effect of Ca^{2+} on the aggregation propensity of SOD1, we have analyzed the variation of the mean light scattering intensity over time (Fig. 3*A*). We determined that the presence of Ca^{2+} promotes an earlier formation of an aggregation nucleus ($t < 48$ h), whereas the onset of aggregation in the control (without Ca^{2+}) occurs substantially later ($t > 70$ h). This suggests that the conformational changes induced by the presence of Ca^{2+} give rise to self-association-prone conformers that promote SOD1 oligomerization under physiological pH. The effect of Ca^{2+} on SOD1 aggregation kinetics was further investigated monitoring binding of thioflavin T, a fluorescent probe that recognizes diverse amyloid-like fibrils and amorphous aggregates (73–76) as well as oligomers and protofibers (77–79). In both cases a sigmoidal-type transition was observed, suggesting a nucleation-dependent aggregation mechanism (Fig. 3*B*). However, Ca^{2+} was shown to impact the aggregation profile of SOD1, namely the lag time and fibrillation rate (Table 1). This was evidenced by a decrease in the time required for the formation of the aggregation nucleus (which was decreased by ~26 h in the presence of Ca^{2+}) and by a decrease in the apparent elongation rate constants.

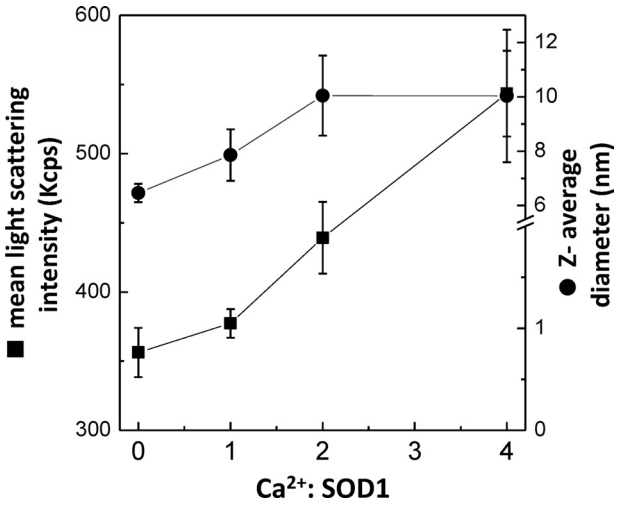

FIGURE 2. **Impact of increasing Ca^{2+} concentrations on apo-SOD1 oligomerization.** DLS analysis (mean size and count rate) of apo-SOD1 upon overnight incubation at 37 °C and stirring, at increasing Ca^{2+}/SOD1 ratios. See "Materials and Methods" for further details. *Error bars*, S.D.

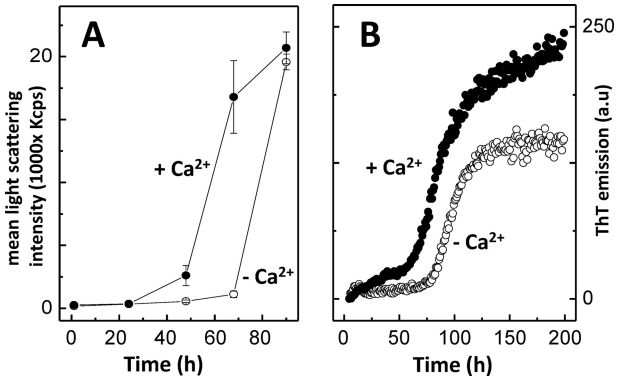

FIGURE 3. **Ca^{2+} enhances apo-SOD1 aggregation.** *A*, aggregation profile of SOD1 monitored by mean light scattering intensity analysis over time, in the absence and in the presence of Ca^{2+}. *B*, aggregation kinetics of SOD1 monitored by ThT fluorescence emission, in the absence and in the presence of Ca^{2+}. $-Ca^{2+}$, no $CaCl_2$; $+Ca^{2+}$, $CaCl_2$/SOD1 = 2. See Table 1 for kinetic parameters and "Materials and Methods" for further details. *Error bars*, S.D.

TABLE 1
Effect of Ca^{2+} on SOD1 aggregation kinetics under physiological pH
Apo-SOD1 aggregation (80 μM) was monitored by ThT fluorescence emission in 50 mM Tris, pH 7.5, with or without Ca^{2+} under 600 rpm agitation with a Teflon bead at 37 °C. ($n = 6$).

Kinetic parameters	$-Ca^{2+}$	$+Ca^{2+}$
t_{lag} (h)	78 ± 12	52 ± 5
t_{50} (h)	98 ± 8	85 ± 8
k_{app} (h^{-1})	0.10 ± 0.03	0.058 ± 0.012

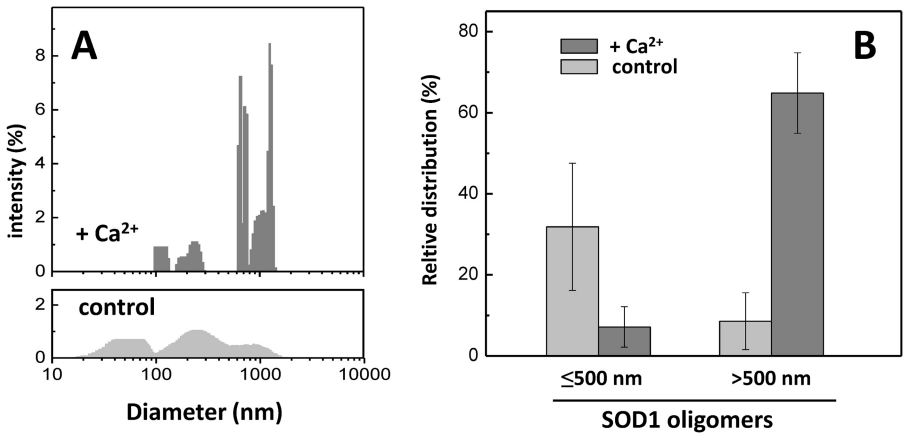

FIGURE 4. **Ca^{2+} favors the formation of larger SOD1 aggregates.** *A*, comparison of the particle size distributions of apo-SOD1 aggregates in the presence (*top*) and in the absence (*bottom*) of Ca^{2+} upon 48-h incubation at 37 °C and stirring. Note the broader distributions at lower particle diameters in the absence of Ca^{2+}. *B*, relative distribution of total light scattering intensities arising from aggregated SOD1 species with a hydrodynamic diameter under and above 500 nm, for the Ca^{2+}-incubated SOD1 and control. $+Ca^{2+}$, $CaCl_2$/SOD1 = 2. See "Materials and Methods" for further details. *Error bars*, S.D.

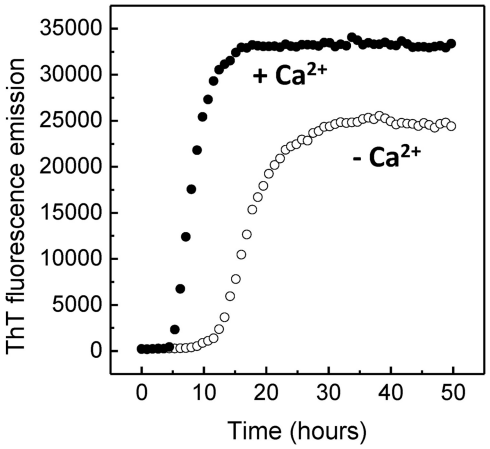

FIGURE 5. **Ca^{2+} enhances apo-SOD1 aggregation also under reducing conditions.** Aggregation kinetics of 80 μM apo-SOD1 with 10 mM tris(2-carboxyethyl)phosphine was monitored by ThT fluorescence emission, in the absence and in the presence of Ca^{2+}. $-Ca^{2+}$, no $CaCl_2$; $+Ca^{2+}$, $CaCl_2$/SOD1 = 2. See Table 2 for kinetic parameters and "Materials and Methods" for further details.

In order to obtain insight into SOD1 oligomers formed at the onset of the exponential phase (t = 48 h), we have compared the particle size distributions (Fig. 4*A*). In the control without calcium, although poorly populated, it is already possible to observe a broad distribution of oligomers (Fig. 4*A*, *bottom*). However, Ca^{2+} populates a pool of larger oligomers (Fig. 4*A*, *top*). Indeed, Ca^{2+} promotes the formation of an increased fraction of larger aggregates (>500 nm), whereas in the control, smaller aggregates (<500 nm) predominate (Fig. 4*B*).

The effect of Ca^{2+} on SOD1 aggregation was also investigated under reducing conditions, a well established factor known to hasten SOD1 aggregation (28, 80) (Fig. 5). A similar effect is observed with respect to non-reducing conditions; further, with a reductant, Ca^{2+} also lowers SOD1 critical concentration for aggregation (Table 2). In summary, the presence of Ca^{2+} potentiates SOD1 aggregation, and this effect is observed irrespective of the redox status of the intramolecular disulfide bond (Cys^{57}–Cys^{146}).

Calcium Influences the Secondary Structure of SOD1 Aggregates—We have also examined the difference ATR-FTIR spectra to probe for conformational changes on SOD1 aggregates formed in the presence of Ca^{2+} (Fig. 6). Ca^{2+} aggregates display prominent β-sheet components at 1630 and 1695 cm^{-1}, likely to be associated with intermolecular antiparallel arrangements of the β-strands, because antiparallel β-sheets exhibit a strong band near ~1630 cm^{-1} and a weaker band near ~1990 cm^{-1} (81–83). On the other hand, in the control, a main β-sheet contribution at 1640 cm^{-1} is observed that can be attributed either to parallel β-sheets or to twisted antiparallel β-sheet structures, because both types of structure have absorption frequencies shifted to higher wave numbers than the corresponding antiparallel β-sheets and often exhibit a reduced/negligible high wave number side band (84). Moreover, Ca^{2+} aggregates have a high content of intermolecular β-sheets (band at 1612 cm^{-1}) (85) as well as β-turns (bands at 1678 and 1664 cm^{-1}); on the other hand, the control denotes a higher content of random structures, as evidenced by the 1655 cm^{-1} negative band.

Calcium Influences the Morphology of SOD1 Aggregate—Having established that Ca^{2+} modulates the secondary structure of SOD1 aggregates, we moved to investigate their morphological differences. For this purpose, we have used conformational antibodies in combination with TEM. The conformational antibodies A11 and OC recognize generic epitopes of soluble oligomers and fibrils, within amyloid proteins, respectively (86, 87). Dot blot analysis of SOD1 aggregates obtained after the plateau phase of the aggregation kinetics was reached (t ~200 h) showed that these are immunoreactive toward both antibodies, indicating that SOD1 aggregates comprise amyloid epitopes (Fig. 7). Interestingly, incubation with Ca^{2+} results in different binding patterns; the presence of Ca^{2+} increases the reactivity toward oligomers (A11) while simultaneously decreasing proportionally the immune response toward fibrils (OC). This result implies that Ca^{2+} decreases the extent of fibril formation, suggesting that the aggregation pathway is diverted toward amorphous aggregates.

The morphology of the aggregates was further investigated using TEM (Fig. 8). In the absence of Ca^{2+}, SOD1 forms amy-

TABLE 2

Effect of Ca^{2+} on apo-SOD aggregation kinetics under reducing conditions

Apo-SOD1 aggregation was monitored by ThT fluorescence emission in 50 mM Tris, pH 7.5, plus 10 mM tris(2-carboxyethyl)phosphine with or without a 2 molar ratio concentration of Ca_2Cl under agitation (600 rpm) with a Teflon bead at 37 °C. NF, no fibrillation observed. See "Materials and Methods" for further details.

	$-Ca^2$			$+Ca^2$		
[SOD1]	t_{lag}	t_{50}	k_{app}	t_{lag}	t_{50}	k_{app}
μM	*h*	*h*	h^{-1}	*h*	*h*	h^{-1}
20	NF	NF	NF	16 ± 3	23 ± 5	0.29 ± 0.12
40	12 ± 4	23 ± 5	0.16 ± 0.08	7 ± 2	12 ± 3	0.4 ± 0.01
80	13 ± 4	17 ± 4	0.41 ± 0.11	6 ± 2	8 ± 4	0.73 ± 0.14
120	8 ± 2	12 ± 3	0.42 ± 0.02	11 ± 4	17 ± 6	0.33 ± 0.22

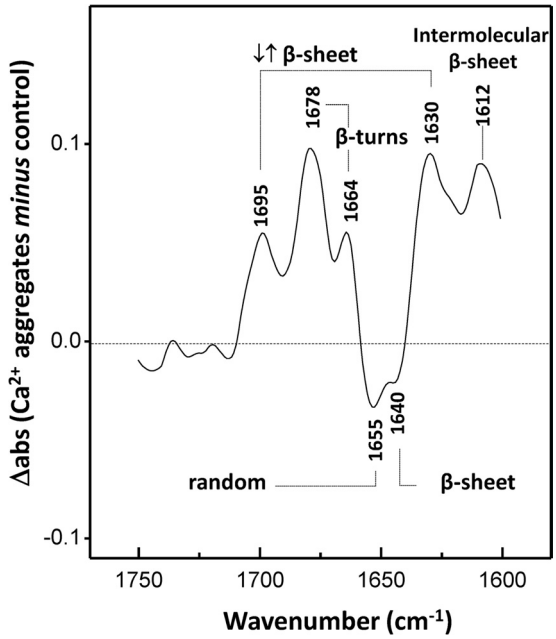

FIGURE 6. **Ca^{2+} induces secondary structure changes on SOD1 aggregates.** ATR-FTIR difference spectrum in the amide I region of SOD1 aggregates formed in the presence of Ca^{2+} minus in its absence. Positive peaks denote features that are enriched by the presence of Ca^{2+}, whereas negative peaks denote structures preferentially formed in the absence of Ca^{2+}. The analyzed aggregates were obtained at pH 7.5 after incubation under constant agitation with a Teflon bead at 37 °C for 150 h. $-Ca^{2+}$, no $CaCl_2$; $+Ca^{2+}$, $CaCl_2$/SOD1 = 2. See "Materials and Methods" for further details.

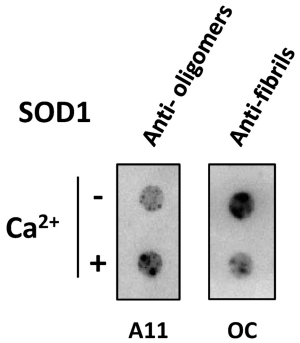

FIGURE 7. **Ca^{2+} influences SOD1 aggregation pathway toward non-fibrillar aggregates.** Shown is dot blot analysis using conformational antibodies. Anti-amyloid oligomer (A11) and anti-amyloid fibril (OC) antibodies were used to test conformers prevalent in SOD1 aggregates formed in the presence and absence of Ca^{2+} ($n = 3$). $-Ca^{2+}$, no $CaCl_2$; $+Ca^{2+}$, $CaCl_2$/SOD1 = 2. See "Materials and Methods" for further details.

loid-like fibrils with characteristic ultrastructural properties with an approximate diameter of 10 nm and several μm in length. In the presence of Ca^{2+}, fibrils still formed, but they were shorter and less abundant (Fig. 8, *bottom panels*). Furthermore, other species were present, namely amorphous aggregates (Fig. 8, *bottom right panel*, *arrow*) and oligomers of different sizes (Fig. 8, *bottom panels*, *arrowheads*), thus forming a more heterogeneous sample. These results fully agree with those obtained using conformational antibodies. TEM observations suggest that Ca^{2+} interfered with SOD1 fibrillogenesis but did not avoid the generation of intermediate amyloidogenic species, such as oligomers and fibrillar aggregates. Thus, the preferential non-fibrillar aggregates and oligomers that are formed by the presence of Ca^{2+} retain the ability to bind ThT and accounted for most of the intensity observed in this assay (Fig. 1*C*). Interestingly, electron microscopy of Lewy body-like SOD1-enriched inclusions from the spinal cord of an ALS mouse model revealed that its core consisted of a heterogeneous mass of tangled filamentous material covered with small granules (14, 88, 89). This suggests that SOD1 inclusions *in vivo* are composed of protein aggregates with heterogeneous mor-

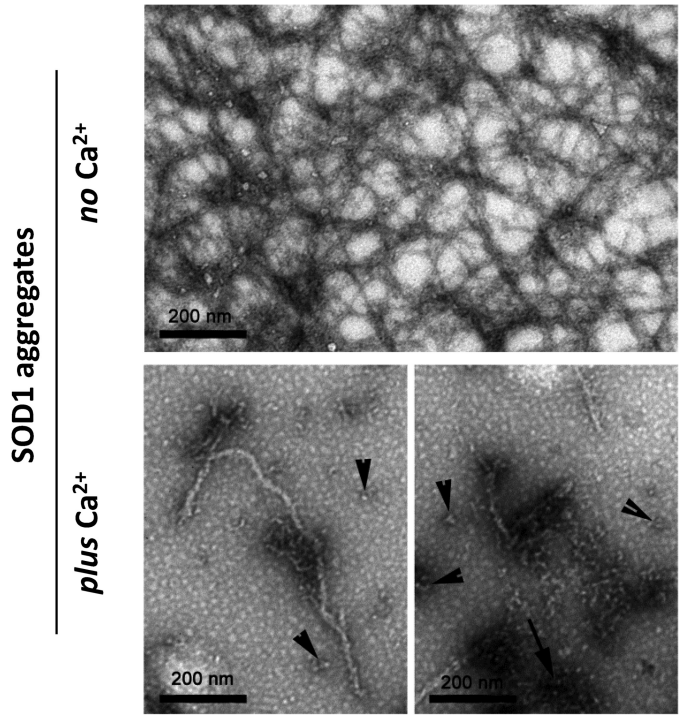

FIGURE 8. **Ca^{2+} modulates the morphology of SOD1 aggregates, as analyzed by TEM.** In the absence of Ca^{2+}, apo-SOD1 formed typical amyloid fibrils with diameters of ~10 nm (*top*). In the presence of Ca^{2+}, fibrils are less abundant; in particular, amorphous aggregates (*bottom right panel*, *arrow*) and oligomers of variable sizes (*bottom panels*, *arrowheads*) were often visualized. Analyzed aggregates derived from apo-SOD1 incubated at pH 7.5 with or without Ca^{2+} under constant agitation with a Teflon bead at 37 °C for 150 h. $-Ca^{2+}$, no $CaCl_2$; $+Ca^{2+}$, $CaCl_2$/SOD1 = 2. See "Materials and Methods" for further details.

phologies, like the ones here found to be formed *in vitro* in the presence of Ca^{2+}.

DISCUSSION

Ca^{2+} is increased in ALS and is particularly abundant in the specific motor neurons affected in this disease, where SOD1-enriched proteinaceous inclusions are found. As a ligand, Ca^{2+} is particularly versatile because it binds sites with irregular geometry, thus facilitating its nonspecific association to proteins (90, 91). In agreement, a bound Ca^{2+} was described in a crystal structure of an SOD1 clinical mutant (92) although sequence analysis and bioinformatics failed to identify any canonical Ca^{2+} binding motif within SOD1. Here we have assayed the effect of Ca^{2+} on the SOD1 aggregation mechanism. Overall, the results obtained show that under physiological pH, Ca^{2+} induces conformational changes on the SOD1 fold that increase its propensity to aggregate. Specifically, Ca^{2+} increases SOD1 β-sheet content and hydrophobicity, which are features likely to result in favorable intramolecular interactions leading to the formation of aggregates (93, 94). Indeed, the presence of Ca^{2+} was shown to promote SOD1 aggregation, both under oxidizing and reducing conditions, diverting the aggregation pathway toward non-fibrillar aggregates and oligomers instead of fibrils. Recent literature suggests that amorphous rather than amyloid-type aggregates are found in SOD1-ALS patient tissue (95), and the reported effects of Ca^{2+} would go along these lines, but this is still a matter of debate in the field (96, 97). This modulation effect by a metal ion has also been demonstrated for other proteins involved in neurodegenerative disorders, highlighting the influence of the chemical neuronal environment with respect to metal ion homeostasis in pathologic aggregation processes (98). Interestingly, Ca^{2+} can also induce α-synuclein aggregation, as shown by cell culture and *in vitro* studies (99–101). This evidence is particularly relevant because pathologic α-synuclein accumulation in Parkinson disease selectively affects dopaminergic neurons that are particularly vulnerable to Ca^{2+} dyshomeostasis, correlating calcium overload with the onset of the disease (102–105). Also, in the case of SOD1, the observed effect of Ca^{2+} can have a particularly meaningful physiological relevance because SOD1 only undergoes aggregation within specific neuron cells of ALS patients (38, 39) that simultaneously show Ca^{2+} overload (47–53). Moreover, it was recently reported that calcium overload in the cytoplasm of cultured motor neurons expressing an ALS-associated mutant promotes SOD1 aggregation into inclusions. Importantly, Ca^{2+} increase is suggested not to be a consequence of SOD1 aggregation because the rise in Ca^{2+} levels in these cells occurs prior to the formation of SOD1 inclusions (54, 55). In any case, SOD1 aggregates promote a further increase in the levels of cytosolic Ca^{2+} (55). In agreement, increasing the Ca^{2+} load exacerbates the insolubility and toxicity of a SOD1 clinical variant (106–109). On the other hand, an opposite effect is observed when Ca^{2+} buffering in cellular and animal models of fALS is increased, which resulted in a protective effect toward aggregation (110–112). Our study provides *in vitro* evidence supporting the hypothesis that Ca^{2+} overload in ALS can actually play a role in SOD1 deposition. Nevertheless, there must be other factors involved in SOD1 aggregation because otherwise SOD1 would probably also aggregate on dopaminergic neurons, which are neurons that feature high levels of labile cytosolic calcium.

Acknowledgments—We thank M. J. Saraiva (IBMC, Portugal) and R. Fernandes (Histology and Electron Microscopy Service, Instituto Biologia Molecular e Celular, Portugal) for assistance with TEM analysis. We gratefully acknowledge M. Oliveberg (Stockholm University) for the SOD1 plasmid.

REFERENCES

1. Rowland, L. P., and Shneider, N. A. (2001) Amyotrophic lateral sclerosis. *N. Engl. J. Med.* **344,** 1688–1700
2. Talbot, K., and Ansorge, O. (2006) Recent advances in the genetics of amyotrophic lateral sclerosis and frontotemporal dementia. Common pathways in neurodegenerative disease. *Hum. Mol. Genet.* **15,** R182–R187
3. Watanabe, M., Dykes-Hoberg, M., Culotta, V. C., Price, D. L., Wong, P. C., and Rothstein, J. D. (2001) Histological evidence of protein aggregation in mutant SOD1 transgenic mice and in amyotrophic lateral sclerosis neural tissues. *Neurobiol. Dis.* **8,** 933–941
4. Bruijn, L. I., Houseweart, M. K., Kato, S., Anderson, K. L., Anderson, S. D., Ohama, E., Reaume, A. G., Scott, R. W., and Cleveland, D. W. (1998) Aggregation and motor neuron toxicity of an ALS-linked SOD1 mutant independent from wild-type SOD1. *Science* **281,** 1851–1854
5. Johnston, J. A., Dalton, M. J., Gurney, M. E., and Kopito, R. R. (2000) Formation of high molecular weight complexes of mutant Cu, Zn-superoxide dismutase in a mouse model for familial amyotrophic lateral sclerosis. *Proc. Natl. Acad. Sci. U.S.A.* **97,** 12571–12576
6. Prudencio, M., Hart, P. J., Borchelt, D. R., and Andersen, P. M. (2009) Variation in aggregation propensities among ALS-associated variants of SOD1. Correlation to human disease. *Hum. Mol. Genet.* **18,** 3217–3226
7. Kato, S., Takikawa, M., Nakashima, K., Hirano, A., Cleveland, D. W., Kusaka, H., Shibata, N., Kato, M., Nakano, I., and Ohama, E. (2000) New consensus research on neuropathological aspects of familial amyotrophic lateral sclerosis with superoxide dismutase 1 (SOD1) gene mutations. Inclusions containing SOD1 in neurons and astrocytes. *Amyotroph. Lateral Scler. Other Motor Neuron Disord.* **1,** 163–184
8. Rosen, D. R., Siddique, T., Patterson, D., Figlewicz, D. A., Sapp, P., Hentati, A., Donaldson, D., Goto, J., O'Regan, J. P., and Deng, H. X. (1993) Mutations in Cu/Zn superoxide dismutase gene are associated with familial amyotrophic lateral sclerosis. *Nature* **362,** 59–62
9. Valentine, J. S., Doucette, P. A., and Zittin Potter, S. (2005) Copper-zinc superoxide dismutase and amyotrophic lateral sclerosis. *Annu. Rev. Biochem.* **74,** 563–593
10. Stieber, A., Gonatas, J. O., and Gonatas, N. K. (2000) Aggregates of mutant protein appear progressively in dendrites, in periaxonal processes of oligodendrocytes, and in neuronal and astrocytic perikarya of mice expressing the SOD1(G93A) mutation of familial amyotrophic lateral sclerosis. *J. Neurol. Sci.* **177,** 114–123
11. Sasaki, S., Warita, H., Murakami, T., Shibata, N., Komori, T., Abe, K., Kobayashi, M., and Iwata, M. (2005) Ultrastructural study of aggregates in the spinal cord of transgenic mice with a G93A mutant SOD1 gene. *Acta Neuropathol.* **109,** 247–255
12. Forsberg, K., Jonsson, P. A., Andersen, P. M., Bergemalm, D., Graffmo, K. S., Hultdin, M., Jacobsson, J., Rosquist, R., Marklund, S. L., and Bränström, T. (2010) Novel antibodies reveal inclusions containing non-native SOD1 in sporadic ALS patients. *PLoS One* **5,** e11552
13. Forsberg, K., Andersen, P. M., Marklund, S. L., and Brännstrom, T. (2011) Glial nuclear aggregates of superoxide dismutase-1 are regularly present in patients with amyotrophic lateral sclerosis. *Acta Neuropathol.* **121,** 623–634
14. Shibata, N., Hirano, A., Kobayashi, M., Sasaki, S., Kato, T., Matsumoto, S., Shiozawa, Z., Komori, T., Ikemoto, A., and Umahara, T. (1994) Cu/Zn superoxide dismutase-like immunoreactivity in Lewy body-like inclu-

sions of sporadic amyotrophic lateral sclerosis. *Neurosci. Lett.* **179,** 149–152
15. Shibata, N., Asayama, K., Hirano, A., and Kobayashi, M. (1996) Immunohistochemical study on superoxide dismutases in spinal cords from autopsied patients with amyotrophic lateral sclerosis. *Dev. Neurosci.* **18,** 492–498
16. Guareschi, S., Cova, E., Cereda, C., Ceroni, M., Donetti, E., Bosco, D. A., Trotti, D., and Pasinelli, P. (2012) An overoxidized form of superoxide dismutase found in sporadic amyotrophic lateral sclerosis with bulbar onset shares a toxic mechanism with mutant SOD1. *Proc. Natl. Acad. Sci. U.S.A.* **109,** 5074–5079
17. Bosco, D. A., Morfini, G., Karabacak, N. M., Song, Y., Gros-Louis, F., Pasinelli, P., Goolsby, H., Fontaine, B. A., Lemay, N., McKenna-Yasek, D., Frosch, M. P., Agar, J. N., Julien, J. P., Brady, S. T., and Brown, R. H., Jr. (2010) Wild-type and mutant SOD1 share an aberrant conformation and a common pathogenic pathway in ALS. *Nat. Neurosci.* **13,** 1396–1403
18. Yates, D. (2010) Motor neuron disease. Misfolded wild-type SOD1 may link sporadic and familial ALS. *Nat. Rev. Neurol.* **6,** 645
19. Wang, J., Slunt, H., Gonzales, V., Fromholt, D., Coonfield, M., Copeland, N. G., Jenkins, N. A., and Borchelt, D. R. (2003) Copper-binding-site-null SOD1 causes ALS in transgenic mice. Aggregates of non-native SOD1 delineate a common feature. *Hum. Mol. Genet.* **12,** 2753–2764
20. Kabashi, E., Valdmanis, P. N., Dion, P., and Rouleau, G. A. (2007) Oxidized/misfolded superoxide dismutase-1. The cause of all amyotrophic lateral sclerosis? *Ann. Neurol.* **62,** 553–559
21. Gruzman, A., Wood, W. L., Alpert, E., Prasad, M. D., Miller, R. G., Rothstein, J. D., Bowser, R., Hamilton, R., Wood, T. D., Cleveland, D. W., Lingappa, V. R., and Liu, J. (2007) Common molecular signature in SOD1 for both sporadic and familial amyotrophic lateral sclerosis. *Proc. Natl. Acad. Sci. U.S.A.* **104,** 12524–12529
22. Haidet-Phillips, A. M., Hester, M. E., Miranda, C. J., Meyer, K., Braun, L., Frakes, A., Song, S., Likhite, S., Murtha, M. J., Foust, K. D., Rao, M., Eagle, A., Kammesheidt, A., Christensen, A., Mendell, J. R., Burghes, A. H., and Kaspar, B. K. (2011) Astrocytes from familial and sporadic ALS patients are toxic to motor neurons. *Nat. Biotechnol.* **29,** 824–828
23. Jonsson, P. A., Graffmo, K. S., Andersen, P. M., Brännström, T., Lindberg, M., Oliveberg, M., and Marklund, S. L. (2006) Disulphide-reduced superoxide dismutase-1 in CNS of transgenic amyotrophic lateral sclerosis models. *Brain* **129,** 451–464
24. Lelie, H. L., Liba, A., Bourassa, M. W., Chattopadhyay, M., Chan, P. K., Gralla, E. B., Miller, L. M., Borchelt, D. R., Valentine, J. S., and Whitelegge, J. P. (2011) Copper and zinc metallation status of copper-zinc superoxide dismutase from amyotrophic lateral sclerosis transgenic mice. *J. Biol. Chem.* **286,** 2795–2806
25. Rumfeldt, J. A., Lepock, J. R., and Meiering, E. M. (2009) Unfolding and folding kinetics of amyotrophic lateral sclerosis-associated mutant Cu,Zn superoxide dismutases. *J. Mol. Biol.* **385,** 278–298
26. Banci, L., Bertini, I., Durazo, A., Girotto, S., Gralla, E. B., Martinelli, M., Valentine, J. S., Vieru, M., and Whitelegge, J. P. (2007) Metal-free superoxide dismutase forms soluble oligomers under physiological conditions. A possible general mechanism for familial ALS. *Proc. Natl. Acad. Sci. U.S.A.* **104,** 11263–11267
27. Teilum, K., Smith, M. H., Schulz, E., Christensen, L. C., Solomentsev, G., Oliveberg, M., and Akke, M. (2009) Transient structural distortion of metal-free Cu/Zn superoxide dismutase triggers aberrant oligomerization. *Proc. Natl. Acad. Sci. U.S.A.* **106,** 18273–18278
28. Chattopadhyay, M., Durazo, A., Sohn, S. H., Strong, C. D., Gralla, E. B., Whitelegge, J. P., and Valentine, J. S. (2008) Initiation and elongation in fibrillation of ALS-linked superoxide dismutase. *Proc. Natl. Acad. Sci. U.S.A.* **105,** 18663–18668
29. Furukawa, Y., and O'Halloran, T. V. (2006) Posttranslational modifications in Cu,Zn-superoxide dismutase and mutations associated with amyotrophic lateral sclerosis. *Antioxid. Redox. Signal.* **8,** 847–867
30. Hörnberg, A., Logan, D. T., Marklund, S. L., and Oliveberg, M. (2007) The coupling between disulphide status, metallation and dimer interface strength in Cu/Zn superoxide dismutase. *J. Mol. Biol.* **365,** 333–342
31. Strange, R. W., Antonyuk, S., Hough, M. A., Doucette, P. A., Rodriguez, J. A., Hart, P. J., Hayward, L. J., Valentine, J. S., and Hasnain, S. S. (2003) The structure of holo and metal-deficient wild-type human Cu, Zn superoxide dismutase and its relevance to familial amyotrophic lateral sclerosis. *J. Mol. Biol.* **328,** 877–891
32. Banci, L., Bertini, I., Cramaro, F., Del Conte, R., and Viezzoli, M. S. (2003) Solution structure of Apo Cu,Zn superoxide dismutase. Role of metal ions in protein folding. *Biochemistry* **42,** 9543–9553
33. Assfalg, M., Banci, L., Bertini, I., Turano, P., and Vasos, P. R. (2003) Superoxide dismutase folding/unfolding pathway. Role of the metal ions in modulating structural and dynamical features. *J. Mol. Biol.* **330,** 145–158
34. Lindberg, M. J., Normark, J., Holmgren, A., and Oliveberg, M. (2004) Folding of human superoxide dismutase. Disulfide reduction prevents dimerization and produces marginally stable monomers. *Proc. Natl. Acad. Sci. U.S.A.* **101,** 15893–15898
35. Arnesano, F., Banci, L., Bertini, I., Martinelli, M., Furukawa, Y., and O'Halloran, T. V. (2004) The unusually stable quaternary structure of human Cu,Zn-superoxide dismutase 1 is controlled by both metal occupancy and disulfide status. *J. Biol. Chem.* **279,** 47998–48003
36. Rodriguez, J. A., Shaw, B. F., Durazo, A., Sohn, S. H., Doucette, P. A., Nersissian, A. M., Faull, K. F., Eggers, D. K., Tiwari, A., Hayward, L. J., and Valentine, J. S. (2005) Destabilization of apoprotein is insufficient to explain Cu,Zn-superoxide dismutase-linked ALS pathogenesis. *Proc. Natl. Acad. Sci. U.S.A.* **102,** 10516–10521
37. Vassall, K. A., Stubbs, H. R., Primmer, H. A., Tong, M. S., Sullivan, S. M., Sobering, R., Srinivasan, S., Briere, L. A., Dunn, S. D., Colón, W., and Meiering, E. M. (2011) Decreased stability and increased formation of soluble aggregates by immature superoxide dismutase do not account for disease severity in ALS. *Proc. Natl. Acad. Sci. U.S.A.* **108,** 2210–2215
38. Cleveland, D. W., and Rothstein, J. D. (2001) From Charcot to Lou Gehrig. Deciphering selective motor neuron death in ALS. *Nat. Rev. Neurosci.* **2,** 806–819
39. Wang, J., Xu, G., and Borchelt, D. R. (2002) High molecular weight complexes of mutant superoxide dismutase 1. Age-dependent and tissue-specific accumulation. *Neurobiol. Dis.* **9,** 139–148
40. Vandenberghe, W., Robberecht, W., and Brorson, J. R. (2000) AMPA receptor calcium permeability, GluR2 expression, and selective motoneuron vulnerability. *J. Neurosci.* **20,** 123–132
41. Shaw, P. J., and Eggett, C. J. (2000) Molecular factors underlying selective vulnerability of motor neurons to neurodegeneration in amyotrophic lateral sclerosis. *J. Neurol.* **247,** I17–I27
42. Williams, T. L., Day, N. C., Ince, P. G., Kamboj, R. K., and Shaw, P. J. (1997) Calcium-permeable α-amino-3-hydroxy-5-methyl-4-isoxazole propionic acid receptors. A molecular determinant of selective vulnerability in amyotrophic lateral sclerosis. *Ann. Neurol.* **42,** 200–207
43. Van Den Bosch, L., Vandenberghe, W., Klaassen, H., Van Houtte, E., and Robberecht, W. (2000) Ca^{2+}-permeable AMPA receptors and selective vulnerability of motor neurons. *J. Neurol. Sci.* **180,** 29–34
44. Guatteo, E., Carunchio, I., Pieri, M., Albo, F., Canu, N., Mercuri, N. B., and Zona, C. (2007) Altered calcium homeostasis in motor neurons following AMPA receptor but not voltage-dependent calcium channels' activation in a genetic model of amyotrophic lateral sclerosis. *Neurobiol. Dis.* **28,** 90–100
45. Alexianu, M. E., Ho, B. K., Mohamed, A. H., La Bella, V., Smith, R. G., and Appel, S. H. (1994) The role of calcium-binding proteins in selective motoneuron vulnerability in amyotrophic lateral sclerosis. *Ann. Neurol.* **36,** 846–858
46. Palecek, J., Lips, M. B., and Keller, B. U. (1999) Calcium dynamics and buffering in motoneurones of the mouse spinal cord. *J. Physiol.* **520,** 485–502
47. Siklós, L., Engelhardt, J. I., Alexianu, M. E., Gurney, M. E., Siddique, T., and Appel, S. H. (1998) Intracellular calcium parallels motoneuron degeneration in SOD-1 mutant mice. *J. Neuropathol. Exp. Neurol.* **57,** 571–587
48. von Lewinski, F., Fuchs, J., Vanselow, B. K., and Keller, B. U. (2008) Low Ca^{2+} buffering in hypoglossal motoneurons of mutant SOD1 (G93A) mice. *Neurosci. Lett.* **445,** 224–228
49. Jaiswal, M. K., and Keller, B. U. (2009) Cu/Zn superoxide dismutase typical for familial amyotrophic lateral sclerosis increases the vulnerabil-

ity of mitochondria and perturbs Ca^{2+} homeostasis in SOD1G93A mice. *Mol. Pharmacol.* **75,** 478–489
50. Bilsland, L. G., Nirmalananthan, N., Yip, J., Greensmith, L., and Duchen, M. R. (2008) Expression of mutant SOD1 in astrocytes induces functional deficits in motoneuron mitochondria. *J. Neurochem.* **107,** 1271–1283
51. Kawamata, H., and Manfredi, G. (2010) Mitochondrial dysfunction and intracellular calcium dysregulation in ALS. *Mech. Ageing Dev.* **131,** 517–526
52. Siklós, L., Engelhardt, J., Harati, Y., Smith, R. G., Joó, F., and Appel, S. H. (1996) Ultrastructural evidence for altered calcium in motor nerve terminals in amyotropic lateral sclerosis. *Ann. Neurol.* **39,** 203–216
53. Grosskreutz, J., Van Den Bosch, L., and Keller, B. U. (2010) Calcium dysregulation in amyotrophic lateral sclerosis. *Cell Calcium* **47,** 165–174
54. Tateno, M., Sadakata, H., Tanaka, M., Itohara, S., Shin, R. M., Miura, M., Masuda, M., Aosaki, T., Urushitani, M., Misawa, H., and Takahashi, R. (2004) Calcium-permeable AMPA receptors promote misfolding of mutant SOD1 protein and development of amyotrophic lateral sclerosis in a transgenic mouse model. *Hum. Mol. Genet.* **13,** 2183–2196
55. Tradewell, M. L., Cooper, L. A., Minotti, S., and Durham, H. D. (2011) Calcium dysregulation, mitochondrial pathology and protein aggregation in a culture model of amyotrophic lateral sclerosis. Mechanistic relationship and differential sensitivity to intervention. *Neurobiol. Dis.* **42,** 265–275
56. Vanselow, B. K., and Keller, B. U. (2000) Calcium dynamics and buffering in oculomotor neurones from mouse that are particularly resistant during amyotrophic lateral sclerosis (ALS)-related motoneurone disease. *J. Physiol.* **525,** 433–445
57. Ahl, I. M., Lindberg, M. J., and Tibell, L. A. (2004) Coexpression of yeast copper chaperone (yCCS) and CuZn-superoxide dismutases in *Escherichia coli* yields protein with high copper contents. *Protein Expr. Purif.* **37,** 311–319
58. Potter, S. Z., Zhu, H., Shaw, B. F., Rodriguez, J. A., Doucette, P. A., Sohn, S. H., Durazo, A., Faull, K. F., Gralla, E. B., Nersissian, A. M., and Valentine, J. S. (2007) Binding of a single zinc ion to one subunit of copper-zinc superoxide dismutase apoprotein substantially influences the structure and stability of the entire homodimeric protein. *J. Am. Chem. Soc.* **129,** 4575–4583
59. Säbel, C. E., Neureuther, J. M., and Siemann, S. (2010) A spectrophotometric method for the determination of zinc, copper, and cobalt ions in metalloproteins using Zincon. *Anal. Biochem.* **397,** 218–226
60. Barth, A., and Zscherp, C. (2002) What vibrations tell us about proteins. *Q. Rev. Biophys.* **35,** 369–430
61. Banci, L., Bertini, I., D'Amelio, N., Gaggelli, E., Libralesso, E., Matecko, I., Turano, P., and Valentine, J. S. (2005) Fully metallated S134N Cu,Zn-superoxide dismutase displays abnormal mobility and intermolecular contacts in solution. *J. Biol. Chem.* **280,** 35815–35821
62. Chiti, F., Taddei, N., Baroni, F., Capanni, C., Stefani, M., Ramponi, G., and Dobson, C. M. (2002) Kinetic partitioning of protein folding and aggregation. *Nat. Struct. Biol.* **9,** 137–143
63. Semisotnov, G. V., Rodionova, N. A., Razgulyaev, O. I., Uversky, V. N., Gripas', A. F., and Gilmanshin, R. I. (1991) Study of the "molten globule" intermediate state in protein folding by a hydrophobic fluorescent probe. *Biopolymers* **31,** 119–128
64. Cardamone, M., and Puri, N. K. (1992) Spectrofluorimetric assessment of the surface hydrophobicity of proteins. *Biochem. J.* **282,** 589–593
65. Tiwari, A., Liba, A., Sohn, S. H., Seetharaman, S. V., Bilsel, O., Matthews, C. R., Hart, P. J., Valentine, J. S., and Hayward, L. J. (2009) Metal deficiency increases aberrant hydrophobicity of mutant superoxide dismutases that cause amyotrophic lateral sclerosis. *J. Biol. Chem.* **284,** 27746–27758
66. Bemporad, F., and Chiti, F. (2012) Protein misfolded oligomers. Experimental approaches, mechanism of formation, and structure-toxicity relationships. *Chem. Biol.* **19,** 315–327
67. Li, Y., Lubchenko, V., and Vekilov, P. G. (2011) The use of dynamic light scattering and brownian microscopy to characterize protein aggregation. *Rev. Sci. Instrum.* **82,** 053106
68. Ferré-D'Amaré, A. R., and Burley, S. K. (1994) Use of dynamic light scattering to assess crystallizability of macromolecules and macromolecular assemblies. *Structure* **2,** 357–359
69. Nobbmann, U., Connah, M., Fish, B., Varley, P., Gee, C., Mulot, S., Chen, J., Zhou, L., Lu, Y., Shen, F., Yi, J., and Harding, S. E. (2007) Dynamic light scattering as a relative tool for assessing the molecular integrity and stability of monoclonal antibodies. *Biotechnol. Genet. Eng. Rev.* **24,** 117–128
70. Montero, M., Alonso, M. T., Carnicero, E., Cuchillo-Ibáñez, I., Albillos, A., García, A. G., García-Sancho, J., and Alvarez, J. (2000) Chromaffin-cell stimulation triggers fast millimolar mitochondrial Ca^{2+} transients that modulate secretion. *Nat. Cell Biol.* **2,** 57–61
71. Tamano, H., and Takeda, A. (2011) Dynamic action of neurometals at the synapse. *Metallomics* **3,** 656–661
72. Franks, K. M., and Sejnowski, T. J. (2002) Complexity of calcium signaling in synaptic spines. *BioEssays* **24,** 1130–1144
73. Hawe, A., Sutter, M., and Jiskoot, W. (2008) Extrinsic fluorescent dyes as tools for protein characterization. *Pharm. Res.* **25,** 1487–1499
74. LeVine, H., 3rd (1999) Quantification of β-sheet amyloid fibril structures with thioflavin T. *Methods Enzymol.* **309,** 274–284
75. LeVine, H., 3rd (1993) Thioflavine T interaction with synthetic Alzheimer's disease β-amyloid peptides. Detection of amyloid aggregation in solution. *Protein Sci.* **2,** 404–410
76. Biancalana, M., and Koide, S. (2010) Molecular mechanism of Thioflavin-T binding to amyloid fibrils. *Biochim. Biophys. Acta* **1804,** 1405–1412
77. Jan, A., Gokce, O., Luthi-Carter, R., and Lashuel, H. A. (2008) The ratio of monomeric to aggregated forms of Aβ40 and Aβ42 is an important determinant of amyloid-β aggregation, fibrillogenesis, and toxicity. *J. Biol. Chem.* **283,** 28176–28189
78. Maezawa, I., Hong, H. S., Liu, R., Wu, C. Y., Cheng, R. H., Kung, M. P., Kung, H. F., Lam, K. S., Oddo, S., Laferla, F. M., and Jin, L. W. (2008) Congo red and thioflavin-T analogs detect Aβ oligomers. *J. Neurochem.* **104,** 457–468
79. Necula, M., Kayed, R., Milton, S., and Glabe, C. G. (2007) Small molecule inhibitors of aggregation indicate that amyloid β oligomerization and fibrillization pathways are independent and distinct. *J. Biol. Chem.* **282,** 10311–10324
80. Oztug Durer, Z. A., Cohlberg, J. A., Dinh, P., Padua, S., Ehrenclou, K., Downes, S., Tan, J. K., Nakano, Y., Bowman, C. J., Hoskins, J. L., Kwon, C., Mason, A. Z., Rodriguez, J. A., Doucette, P. A., Shaw, B. F., and Valentine, J. S. (2009) Loss of metal ions, disulfide reduction and mutations related to familial ALS promote formation of amyloid-like aggregates from superoxide dismutase. *PLoS One* **4,** e5004
81. Chirgadze, Y. N., and Nevskaya, N. A. (1976) Infrared spectra and resonance interaction of amide-I vibration of the paraellel-chain pleated sheets. *Biopolymers* **15,** 627–636
82. Krimm, S., and Bandekar, J. (1986) Vibrational spectroscopy and conformation of peptides, polypeptides, and proteins. *Adv. Protein Chem.* **38,** 181–364
83. van de Weert, M., Haris, P. I., Hennink, W. E., and Crommelin, D. J. (2001) Fourier transform infrared spectrometric analysis of protein conformation. Effect of sampling method and stress factors. *Anal. Biochem.* **297,** 160–169
84. Barth, A. (2007) Infrared spectroscopy of proteins. *Biochim. Biophys. Acta* **1767,** 1073–1101
85. Okuno, A., Kato, M., and Taniguchi, Y. (2006) The secondary structure of pressure- and temperature-induced aggregates of equine serum albumin studied by FT-IR spectroscopy. *Biochim. Biophys. Acta* **1764,** 1407–1412
86. Kayed, R., Head, E., Thompson, J. L., McIntire, T. M., Milton, S. C., Cotman, C. W., and Glabe, C. G. (2003) Common structure of soluble amyloid oligomers implies common mechanism of pathogenesis. *Science* **300,** 486–489
87. Kayed, R., Head, E., Sarsoza, F., Saing, T., Cotman, C. W., Necula, M., Margol, L., Wu, J., Breydo, L., Thompson, J. L., Rasool, S., Gurlo, T., Butler, P., and Glabe, C. G. (2007) Fibril specific, conformation dependent antibodies recognize a generic epitope common to amyloid fibrils and fibrillar oligomers that is absent in prefibrillar oligomers. *Mol. Neurodegener.* **2,** 18

88. Bruijn, L. I., Becher, M. W., Lee, M. K., Anderson, K. L., Jenkins, N. A., Copeland, N. G., Sisodia, S. S., Rothstein, J. D., Borchelt, D. R., Price, D. L., and Cleveland, D. W. (1997) ALS-linked SOD1 mutant G85R mediates damage to astrocytes and promotes rapidly progressive disease with SOD1-containing inclusions. *Neuron* **18,** 327–338
89. Kato, S., Nakashima, K., Horiuchi, S., Nagai, R., Cleveland, D. W., Liu, J., Hirano, A., Takikawa, M., Kato, M., Nakano, I., Sakoda, S., Asayama, K., and Ohama, E. (2001) Formation of advanced glycation end-product-modified superoxide dismutase-1 (SOD1) is one of the mechanisms responsible for inclusions common to familial amyotrophic lateral sclerosis patients with SOD1 gene mutation, and transgenic mice expressing human SOD1 gene mutation. *Neuropathology* **21,** 67–81
90. Berridge, M. J., Bootman, M. D., and Roderick, H. L. (2003) Calcium signalling. Dynamics, homeostasis and remodelling. *Nat. Rev. Mol. Cell Biol.* **4,** 517–529
91. Carafoli, E. (2005) Calcium. A universal carrier of biological signals. Delivered on 3 July 2003 at the Special FEBS Meeting in Brussels. *FEBS J.* **272,** 1073–1089
92. Winkler, D. D., Schuermann, J. P., Cao, X., Holloway, S. P., Borchelt, D. R., Carroll, M. C., Proescher, J. B., Culotta, V. C., and Hart, P. J. (2009) Structural and biophysical properties of the pathogenic SOD1 variant H46R/H48Q. *Biochemistry* **48,** 3436–3447
93. Kundu, B., and Guptasarma, P. (2002) Use of a hydrophobic dye to indirectly probe the structural organization and conformational plasticity of molecules in amorphous aggregates of carbonic anhydrase. *Biochem. Biophys. Res. Commun.* **293,** 572–577
94. Vetri, V., and Militello, V. (2005) Thermal induced conformational changes involved in the aggregation pathways of β-lactoglobulin. *Biophys. Chem.* **113,** 83–91
95. Kerman, A., Liu, H.-N., Croul, S., Bilbao, J., Rogaeva, E., Zinman, L., Robertson, J., and Chakrabartty, A. (2010) Amyotrophic lateral sclerosis is a non-amyloid disease in which extensive misfolding of SOD1 is unique to the familial form. *Acta Neuropathol.* **119,** 335–344
96. Nordlund, A., and Oliveberg, M. (2006) Folding of Cu/Zn superoxide dismutase suggests structural hotspots for gain of neurotoxic function in ALS. Parallels to precursors in amyloid disease. *Proc. Natl. Acad. Sci. U.S.A.* **103,** 10218–10223
97. Sábado, J., Casanovas, A., Hernandez, S., Piedrafita, L., Hereu, M., and Esquerda, J. E. (2013) Immunodetection of disease-associated conformers of mutant Cu/Zn superoxide dismutase 1 selectively expressed in degenerating neurons in amyotrophic lateral sclerosis. *J. Neuropathol. Exp. Neurol.* **72,** 646–661
98. Leal, S. S., Botelho, H. M., and Gomes, C. M. (2012) Metal ions as modulators of protein conformation and misfolding in neurodegeneration. *Coordination Chem. Rev.* **256,** 2253–2270
99. Nath, S., Goodwin, J., Engelborghs, Y., and Pountney, D. L. (2011) Raised calcium promotes α-synuclein aggregate formation. *Mol. Cell Neurosci.* **46,** 516–526
100. Nielsen, M. S., Vorum, H., Lindersson, E., and Jensen, P. H. (2001) Ca^{2+} binding to α-synuclein regulates ligand binding and oligomerization. *J. Biol. Chem.* **276,** 22680–22684
101. Lowe, R., Pountney, D. L., Jensen, P. H., Gai, W. P., and Voelcker, N. H. (2004) Calcium(II) selectively induces α-synuclein annular oligomers via interaction with the C-terminal domain. *Protein Sci.* **13,** 3245–3252
102. Mosharov, E. V., Larsen, K. E., Kanter, E., Phillips, K. A., Wilson, K., Schmitz, Y., Krantz, D. E., Kobayashi, K., Edwards, R. H., and Sulzer, D. (2009) Interplay between cytosolic dopamine, calcium, and α-synuclein causes selective death of substantia nigra neurons. *Neuron* **62,** 218–229
103. Chan, C. S., Guzman, J. N., Ilijic, E., Mercer, J. N., Rick, C., Tkatch, T., Meredith, G. E., and Surmeier, D. J. (2007) "Rejuvenation" protects neurons in mouse models of Parkinson's disease. *Nature* **447,** 1081–1086
104. Surmeier, D. J., Guzman, J. N., and Sanchez-Padilla, J. (2010) Calcium, cellular aging, and selective neuronal vulnerability in Parkinson's disease. *Cell Calcium* **47,** 175–182
105. Surmeier, D. J., Guzman, J. N., Sanchez-Padilla, J., and Schumacker, P. T. (2011) The role of calcium and mitochondrial oxidant stress in the loss of substantia nigra pars compacta dopaminergic neurons in Parkinson's disease. *Neuroscience* **198,** 221–231
106. Kim, H. J., Im, W., Kim, S., Kim, S. H., Sung, J. J., Kim, M., and Lee, K. W. (2007) Calcium-influx increases SOD1 aggregates via nitric oxide in cultured motor neurons. *Exp. Mol. Med.* **39,** 574–582
107. Van Damme, P., Braeken, D., Callewaert, G., Robberecht, W., and Van Den Bosch, L. (2005) GluR2 deficiency accelerates motor neuron degeneration in a mouse model of amyotrophic lateral sclerosis. *J. Neuropathol. Exp. Neurol.* **64,** 605–612
108. Kuner, R., Groom, A. J., Müller, G., Kornau, H. C., Stefovska, V., Bresink, I., Hartmann, B., Tschauner, K., Waibel, S., Ludolph, A. C., Ikonomidou, C., Seeburg, P. H., and Turski, L. (2005) Mechanisms of disease. Motoneuron disease aggravated by transgenic expression of a functionally modified AMPA receptor subunit. *Ann. N.Y. Acad. Sci.* **1053,** 269–286
109. Parone, P. A., Da Cruz, S., Han, J. S., McAlonis-Downes, M., Vetto, A. P., Lee, S. K., Tseng, E., and Cleveland, D. W. (2013) Enhancing mitochondrial calcium buffering capacity reduces aggregation of misfolded SOD1 and motor neuron cell death without extending survival in mouse models of inherited amyotrophic lateral sclerosis. *J. Neurosci.* **33,** 4657–4671
110. Van Den Bosch, L., Van Damme, P., Bogaert, E., and Robberecht, W. (2006) The role of excitotoxicity in the pathogenesis of amyotrophic lateral sclerosis. *Biochim. Biophys. Acta* **1762,** 1068–1082
111. Roy, J., Minotti, S., Dong, L., Figlewicz, D. A., and Durham, H. D. (1998) Glutamate potentiates the toxicity of mutant Cu/Zn-superoxide dismutase in motor neurons by postsynaptic calcium-dependent mechanisms. *J. Neurosci.* **18,** 9673–9684
112. Beers, D. R., Ho, B. K., Siklós, L., Alexianu, M. E., Mosier, D. R., Mohamed, A. H., Otsuka, Y., Kozovska, M. E., McAlhany, R. E., Smith, R. G., and Appel, S. H. (2001) Parvalbumin overexpression alters immune-mediated increases in intracellular calcium, and delays disease onset in a transgenic model of familial amyotrophic lateral sclerosis. *J. Neurochem.* **79,** 499–509